

# Competition between lasing and superradiance under spintronic pumping

Oksana Chelpanova<sup>1</sup>, Alessio Lerose<sup>2</sup>, Shu Zhang<sup>3,4</sup>, Iacopo Carusotto<sup>5</sup>, Yaroslav Tserkovnyak<sup>4</sup>, Jamir Marino<sup>1,6</sup>

<sup>1</sup>*Institut für Physik, Johannes Gutenberg Universität Mainz, D-55099 Mainz, Germany*

<sup>2</sup>*Department of Theoretical Physics, University of Geneva,  
Quai Ernest-Ansermet 30, 1205 Geneva, Switzerland*

<sup>3</sup>*Max-Planck-Institut für Physik komplexer Systeme, 01187 Dresden, Germany*

<sup>4</sup>*Department of Physics and Astronomy, University of California, Los Angeles, CA 90095, USA*

<sup>5</sup>*INO-CNR BEC Center and Dipartimento di Fisica, Università di Trento, 38123 Trento, Italy*

<sup>6</sup>*Kavli Institute for Theoretical Physics, University of California, Santa Barbara, CA 93106, USA*

(Dated: December 10, 2021)

We consider a platform featuring the minimal ingredients relevant both to a driven-dissipative cavity quantum optics system and to a spintronically pumped magnon condensate. We extend the Dicke model for a bosonic mode collectively coupled to a coherent spin ensemble, by weakly coupling it to an out-of-equilibrium spin bath which is tunable by incoherent pumping. Our model exhibits competition between coherent couplings and dissipative channels, which leads to various collective quantum behaviors, static and dynamic, depending on the interplay of spin-boson interactions and spin pump/loss rates. Our analysis exposes a hybrid lasing-superradiant regime which does not take place in an ordinary pumped Dicke spin ensemble. We interpret the resultant non-equilibrium phase diagram from both a quantum optics and a spintronics standpoint, supplying a conceptual bridge between the two fields. The implications of our results concern dynamical control in spintronics and frequency-dependent gain media in quantum optics.

*Introduction.* The theme of dynamical phase transitions enabled by the interplay of interactions, drive, and dissipation permeates different branches of quantum many body physics, such as quantum optics [1], cold atoms [2], and non-equilibrium solid state physics [3, 4]. The interest in them ranges from practical applications in dynamical control to the fundamentals of statistical mechanics. The exploration and understanding of non-equilibrium phases could be advanced by a unifying language, which, however, remains elusive due to the diversity of microscopic ingredients, relevant scales, and engineering capabilities across the various platforms.

In this Letter, we take a first step in filling this gap by studying a barebones model that offers complementary interpretations pertinent both to spintronics and driven-dissipative quantum optics — as illustrated in Fig. 1(a). We analyse a spin ensemble where coherent dynamical responses ascribable to lasing can be induced by weak coupling to a subsystem incoherently pumped into a population inverted regime. The model can be realized in an optical cavity, where two species of atoms,  $\mathcal{S}$  and  $\mathcal{T}$ , are coupled to each other as well as to a common lossy cavity mode [cf. Fig. 1(b)]. The ensemble  $\mathcal{S}$  collectively couples to the cavity photon via a Dicke term, while the ensemble  $\mathcal{T}$  does via a spin-boson interconversion term. Dynamical instabilities can be induced in the subsystem  $\mathcal{S}$  by incoherently spin pumping the subsystem  $\mathcal{T}$ , even in a limit of weak coupling between them. The interplay of the spin pumping and the Dicke coupling opens a parameter space where lasing and superradiant phases compete and lead to novel dynamical regimes exhibiting features of both. The Dicke coupling also gives rise to hybrid light-matter excitations in the form of upper and lower polariton modes [5]. Tuning the spin frequency in  $\mathcal{T}$  to one of these polariton frequencies, we resonantly trigger

a polariton dynamical instability [6] in  $\mathcal{S}$ , therefore using  $\mathcal{T}$  as a frequency-dependent gain medium [7–9].

Our motivation to separate the coherent ( $\mathcal{S}$ ) and incoherent ( $\mathcal{T}$ ) spin subsystems stems from a solid-state viewpoint, to allow quantum correlations to settle in without much disruption from direct pumping processes. Considering magnet-metal heterostructures [10–18] as a primary example, the magnet layer has a stiff order parameter accompanied by coherent excitations [19], while itinerant electrons carrying incoherent spins in the metal layer are more amenable to external control [20]. One of the consequences of the magnet being a strongly interacting system is the propensity of a long-wavelength magnon to undergo (Bose-Einstein) condensation [21–23], which is mimicked by the bosonic mode in our model. In a magnet, such condensation can manifest as a static phase transition [24], or a dynamical one with the magnetic order parameter precessing spontaneously [25–27], bearing analogy to the superradiant and lasing transitions, respectively. As shown in Fig. 1(c), a magnon condensation can be triggered by electrically pumping the heterostructure [28–32], where a spin accumulation is induced via the spin Hall effect in the metal [33–38] and exerts a spin torque [39–41] on the magnetic dynamics to reverse its decay. In addition, the magnon condensate and the thermally occupied short-wavelength magnons undergo coupled dynamics, previously described by a two-fluid theory [42]. Our model, though much simplified from this practical scenario, allows for a full treatment of the interplay of spin pumping, coupling between the interacting magnetic system and pumped reservoir, and dissipative effects.

*Model.* We consider a Dicke sample [43–47], which consists of an ensemble  $\mathcal{S}$  of  $N$  spins-1/2 collectively coupled to a bosonic mode  $a$  of frequency  $\omega_c$ , weakly interacting

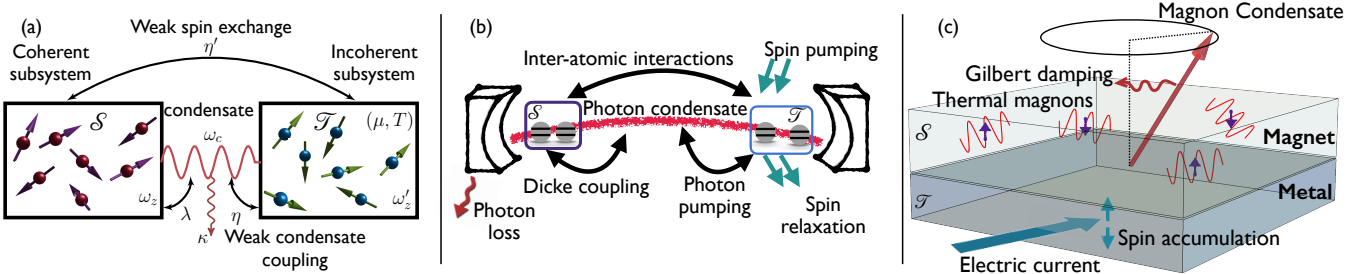


FIG. 1. (a) An ensemble of spins-1/2 ( $\mathcal{S}$ ) is coupled to a bosonic mode (in red) which models a magnon condensate or a cavity boson which can become macroscopically occupied for large values of the Dicke coupling,  $\lambda$ . It is also coupled to a spin-1/2 subsystem ( $\mathcal{T}$ ) under incoherent spin relaxation and pump. When  $\mu > \omega'_z$  the population inversion of  $\mathcal{T}$  can induce a coherent dynamical response in  $\mathcal{S}$ , which is the central mechanism explored in this work. Dissipation with strength  $\kappa$  acts on the bosonic mode and is shown by a red wiggle line. The model contains the essential ingredients of both quantum optics (b) and spintronics (c) platforms, as detailed in the main text.

with an ensemble  $\mathcal{T}$  of an additional set of  $N$  spins. The

level splitting of spins in subsystem  $\mathcal{S}$  ( $\mathcal{T}$ ) is  $\omega_z$  ( $\omega'_z$ ). The full Hamiltonian reads

$$H = \omega_c a^\dagger a + \omega_z \mathcal{S}^z + \omega'_z \mathcal{T}^z + \frac{\lambda}{\sqrt{N}} (a + a^\dagger) (\mathcal{S}^+ + \mathcal{S}^-) + \frac{\eta}{\sqrt{N}} (a \mathcal{T}^+ + a^\dagger \mathcal{T}^-) + \frac{\eta'}{N} (\mathcal{S}^+ \mathcal{T}^- + \mathcal{S}^- \mathcal{T}^+), \quad (1)$$

where  $a$  and  $a^\dagger$  are bosonic annihilation/creation operators, mimicking the magnon condensate or the cavity photon, while the collective spin operators are  $\mathcal{S}^z = \sum_{i=1}^N \sigma_i^z$  and  $\mathcal{T}^z = \sum_{i=1}^N \tau_i^z$ . Here  $\sigma_i^\alpha$  and  $\tau_i^\alpha$  with  $\alpha = x, y, z$  are spin-1/2 operators. We have introduced the Dicke coupling  $\lambda$ , a small boson-spin interconversion term  $\eta$ , and a small spin exchange coupling  $\eta'$ .

The ensemble  $\mathcal{T}$  is driven incoherently into a grand-canonical state with temperature  $T$  and spin accumulation  $\mu$ , by spin pump with rate  $\gamma_\uparrow$  and loss  $\gamma_\downarrow$ , which is described by the following Lindblad master equation [48] for the joint density matrix of the total system:

$$\frac{d\rho}{dt} = -i[H, \rho] + \kappa \mathcal{D}[a] + \gamma_\uparrow \sum_{i=1}^N \mathcal{D}[\tau_i^+ + \gamma_\downarrow \sum_{i=1}^N \mathcal{D}[\tau_i^-], \quad (2)$$

neglecting spin dephasing effects [43]. The dissipators  $\mathcal{D}[x] \equiv x \rho x^\dagger - 1/2 \{x^\dagger x, \rho\}$  are defined as usual, and the spin pump and loss rates  $\gamma_\uparrow = \gamma_t / (1 + e^{\beta(\omega'_z - \mu)})$  and  $\gamma_\downarrow = \gamma_t / (1 + e^{-\beta(\omega'_z - \mu)})$  are parametrized by  $\beta = T^{-1} > 0$  and  $\mu$ , with  $\gamma_t = \gamma_\uparrow + \gamma_\downarrow \geq 0$ . Evolution according to Eq. (2) drives the system into a mixed state with a relative population of up and down spins controlled by the ratio  $\gamma_\uparrow / \gamma_t$ . When  $\mu > \omega'_z$ , the incoherent subsystem  $\mathcal{T}$  experiences population inversion which can be transferred to the rest of the system via  $\eta$  and  $\eta'$  and trigger a lasing instability. For  $\gamma_t \gg \eta, \eta'$ , it quickly relaxes towards a steady state with  $\langle \mathcal{T}^z \rangle \approx (\gamma_\uparrow - \gamma_\downarrow) / 2\gamma_t$ , and  $\langle \mathcal{T}^\pm \rangle \approx 0$ . In presenting results below we use normalized variables  $a \propto a/\sqrt{N}$ ,  $S \propto S/N$ ,  $\mathcal{T} \propto \mathcal{T}/N$ , as customary

in the treatment of systems with collective light-matter interactions [43–45].

*Dissipation.* In the dissipative dynamics of Eq. (2), we have also considered photon loss with rate  $\kappa$  in order to model the photon line-width of the cavity. The relaxation of the collective bosonic mode in a magnet, on the other hand, depends self-consistently on its dynamics [49]. We therefore consider, as alternative, a viscous damping of the magnon condensate, whenever the spintronic relevance is concerned. In terms of magnetic dynamics, the phenomenological Gilbert damping [50] slows down the coherent precession of the order parameter and brings it towards the global equilibrium state [40, 51]. Interestingly, our results remain qualitatively unaltered under dissipation through photon loss or Gilbert damping [52]. Due to the weak coupling to the incoherent ensemble  $\mathcal{T}$ , the photon mode (and the ensemble  $\mathcal{S}$ ) becomes effectively pumped when  $\mathcal{T}$  enters the population inverted state. This results in a reduced effective photon decay rate  $\tilde{\kappa}$ , the sign change of which indicates the onset of dynamical instability.

Before moving to a thorough discussion of our results, we remark that the model in Fig. 1 should not be regarded as a faithful modelization of an actual spintronics system. For instance, the Dicke coupling does not naturally occur in magnets. Rather, it contains the key ingredients for interplay of coherent interactions, spin pumping and magnon damping in a spintronics platform, to reveal the mechanisms for the formation of novel dynamical phases which could then be explored in the future within realistic devices.

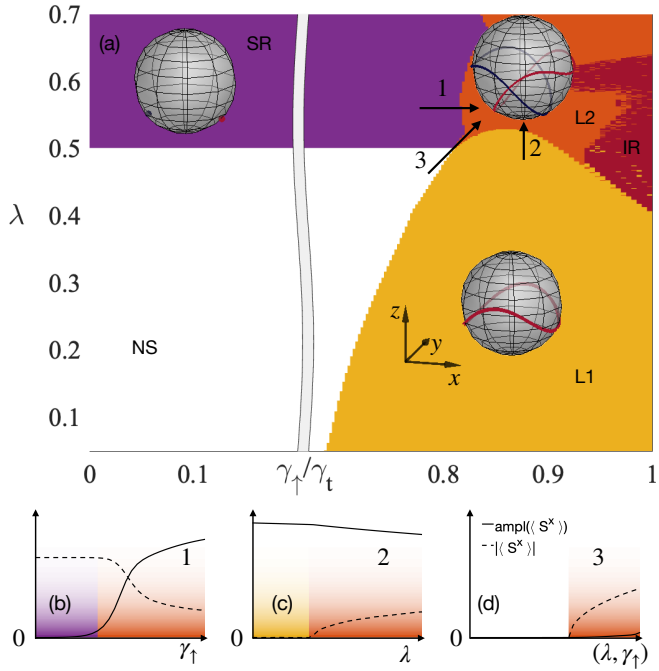


FIG. 2. Dynamical phases resulting from the interplay of spin pumping and Dicke coupling: (a) For  $\gamma_{\uparrow} < \gamma_t/2$ , the usual critical coupling ( $\lambda_c \simeq 0.5$ ) associated to the Dicke transition, separates the normal (NS) from the superradiant (SR) phase. For  $\gamma_{\uparrow} > \gamma_t/2$ , the normal state becomes unstable, and observables in the ensemble  $\mathcal{S}$  oscillate with zero average value of  $\langle S^x \rangle$  in the region L1, and around one of minima of the SR phase in the region L2, as shown in the Bloch spheres. Inside the irregular (IR) region the motion of the collective spin covers uniformly a large part of the Bloch sphere without any structured pattern, and suggestive of chaotic behaviour. Panels (b)–(d) show the absolute value of time-averaged  $\langle S^x \rangle$  (dashed line) and amplitude of its oscillations (solid line) along the transition lines 1, 2 and 3 in the main inset (a). Here we have chosen  $\omega_c = \omega_z = \omega'_z = 1$ ,  $\gamma_t = 1$ ,  $\eta = \eta' = 0.1$ ,  $\kappa = 0.06$ .

*Superradiance and lasing.* We start by revisiting some established dynamical regimes of the hamiltonian in Eq. (1). For  $\eta = \eta' = 0$ , we recover a standard Dicke model [45, 53]. With  $\lambda < \lambda_c = \sqrt{(\omega_z(\omega_c^2 + \kappa^2/4))/4\omega_c}$  the system is in the normal state (NS) with a vanishing  $\langle S^x \rangle$  component and no macroscopic occupation of the photonic mode. By increasing  $\lambda > \lambda_c$  the system enters a super-radiant (SR) phase where it spontaneously breaks  $\mathbb{Z}_2$  symmetry, exhibiting  $\langle S^x \rangle \neq 0$  and photon condensation,  $n = \langle a^\dagger a \rangle \neq 0$ . This picture remains valid when small  $\eta$  and  $\eta'$  are switched on while the spin pumping is kept weak, namely  $\gamma_{\uparrow} < \gamma_t/2$  (cf. Fig. 2(a)).

Another limit  $\eta' = \lambda = 0$  corresponds to the incoherently pumped Tavis-Cummings model [43, 45, 54–57]. The choice trivializes the dynamics of the ensemble  $\mathcal{S}$ . For  $\gamma_{\uparrow}/\gamma_t \geq 1/2 + \kappa\gamma_t/(8\eta^2) + \kappa\gamma_t(\omega_c - \omega'_z)^2/(2\eta^2(\kappa + \gamma_t)^2)$ , the  $\mathcal{T}$  spins experience population inversion, with  $\langle a \rangle$  and  $\langle \mathcal{T}^{x,y} \rangle$  undergoing oscillations. At long times, both  $\langle \mathcal{T}^z \rangle$  and the photon number approach the steady

values set by the pumping rates  $\gamma_{\uparrow/\downarrow}$  [52].

*Dynamical phase diagram.* By turning on  $\lambda$  together with sizeable spin pumping in a weakly coupling limit ( $\eta, \eta' \rightarrow 0^+$ ), we generate the diagram of dynamical responses (cf. Fig. 2) in mean-field treatment, which is exact for  $N \rightarrow \infty$  [45, 58, 59]. In the Supplemental Materials [52] we present the associated equations of motion and also analyze the breakdown of mean field from finite  $N$  corrections.

For strong pumping ( $\gamma_{\uparrow} > \gamma_t/2$ ), the spins in the ensemble  $\mathcal{S}$  display long-lived oscillatory dynamics (see Bloch spheres in Fig. 2). The region L1 in Fig. 2 resembles the regular lasing [55] discussed above, while L2 features 'superradiant' oscillations. The transition from L1 to L2 occurs around values of the Dicke coupling  $\sim \lambda_c$ , with a non-vanishing time average of  $\langle S^x \rangle$  in L2. In this phase we observe persistent oscillatory dynamics reminiscent of lasing around one of the symmetry-broken states of the Dicke model. Such 'superradiant' oscillations would not arise by directly pumping a Dicke model through the Lindblad channels in Eq. (2); they are a result of the pumping scheme of Fig. 1 conceptually borrowed from spintronics. In this regard, the dynamical phase L2 is a conceptual 'bridge' between the quantum optics and spintronics communities which we are aiming to lay out in this work. Notice that despite the pumped subsystem experiences population inversion, the spin ensemble  $\mathcal{S}$  remains in a state with negative  $\langle S^z \rangle$  in both phases L1 and L2.

We now discuss the role of symmetries in the oscillatory dynamics displayed in L1 and L2, and in the transitions between these two different regimes. For  $\lambda = 0$  the photon number  $n$  does not oscillate. A nonzero  $\lambda$  breaks the  $U(1)$  symmetry and the oscillations in  $n$  can be attributed to ellipticity in the spontaneous precession in absence of  $S^z$  conservation. In fact, the dynamics are instead governed by a  $\mathbb{Z}_2$  symmetry, reflected in the observation that the oscillatory frequency of  $n$  and  $\langle S^z \rangle$  is twice that of  $\langle S^x \rangle$ . The transition from L1 to L2 is characterized by an increase in the time-average value of  $\langle S^x \rangle$ , which can be explained by the spontaneous breaking of the  $\mathbb{Z}_2$  symmetry upon increasing the Dicke coupling  $\lambda$  [cf. Fig. 2(c)]. The transition from the SR region to the L2 region appears as a crossover in finite-time numerical data, as the damping of the oscillations of  $\langle S^x \rangle$  critically slows down upon approaching the transition point from the SR side, hence the time-averaged amplitude of the oscillations in a long but finite time windows smoothly grows, blurring the expected singular behavior at the phase boundary [cf. Fig. 2(b)] associated to the dynamical spontaneous symmetry breaking of the  $U(1)$  symmetry. Finally, in the transition from NS to L2, the absolute value of the time average of  $\langle S^x \rangle$ , as well as its amplitude, build up [cf. Fig. 2(d)].

This dynamical phase diagram with competing stationary (NS, SR) and oscillatory (L1, L2, IR) phases is of particular interest to spintronics, since it emerges from the interplay of incoherent spin pumping and ellipticity. The

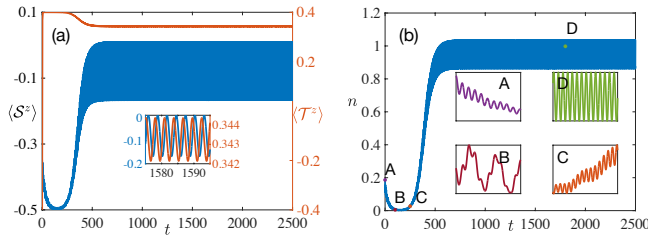


FIG. 3. The left panel shows the dynamics of  $\langle S^z \rangle$  and  $\langle T^z \rangle$  with parameters as in Fig. 2, with the sole exception of  $\omega_z'$  that is now chosen in resonance with the upper polariton frequency ( $\omega_z' \simeq \Omega_U$ ). The system is prepared in the SR state and evolved with system's parameters  $\gamma_\uparrow$  and  $\lambda$  inside the region L1. The right panel shows different stages of the photon number evolution. The initial stage of dynamics is governed by the decaying lower polariton mode, while at stage C the upper polaritonic mode undergoes the dynamical instability triggered by the resonance with the incoherent subsystem; accordingly, the photon number starts to grow until it saturates around times  $t \simeq 500$ . At long times,  $n$  oscillates at the upper polaritonic frequency (panel D). This is illustrative of the spin ensemble  $\mathcal{T}$  acting as a frequency-dependent gain medium.

explicit breaking of U(1) symmetry, which is common for magnets with anisotropies, but largely absent in previous studies of spin-wave lasing [28, 29], suggests richer phenomena accompanying non-equilibrium phase transitions in spintronic devices. Although our model description distillates only the essential mechanisms of an actual spintronics setup, we now briefly discuss some possible implications of our results. The magnon “lasing” [25] in a uniaxial magnet can converge to a steady condensate density featured by a circular precession [28, 29]. Turning on interactions explicitly breaking the U(1) symmetry is expected to induce an ellipticity in the spontaneous precession [60], accompanied by an oscillation of the condensate density due to the absence of spin conservation. This is similar to the dynamics observed in the L1 phase with  $\lambda \neq 0$ . In the regime where both  $\mathbb{Z}_2$  interactions and the pumping effects are sizable, two equivalent  $\mathbb{Z}_2$ -breaking limit cycles are possible (L2 phase). During the electrical pumping, angular momentum transfers reciprocally between the magnet and metal [41]: as the itinerant electrons exert a spin torque to establish the magnon lasing, the coherent magnetic precession simultaneously pumps a spin current back into the metal [61], triggering transverse spin dynamics. Therefore, suppressing the transverse spin dynamics in the metal can be detrimental to magnon lasing, as consistent with the consequence of a fast-relaxing incoherent subsystem discussed above (large  $\gamma_t$  limit).

*Polaritonic lasing.* Observables in the L1 and L2 phases show signatures of upper (U) and lower (L) polaritonic modes [44], which are symmetric (U) and anti-symmetric (L) linear superpositions of spin and photon fields, describing light-matter hybridization via the Dicke coupling  $\lambda$ . In order to appreciate this point, we rewrite the interaction term in (1) as  $H_{int} = (\eta a + \eta' S^-) \mathcal{T}^+ +$

$h.c.$ , which is suggestive of the  $\mathcal{T}$  ensemble pumping a superposition of light and matter excitations into the  $\mathcal{S}$  system. Thus, upper or lower polaritons can be excited in the system, depending whether the two couplings have same or opposite sign, jointly with the resonance condition,  $\omega_z' \simeq \Omega_{U/L}$  (for related expressions, cf. [52]). The effective decay rates of the two polariton modes depend on the frequency of the incoherent subsystem  $\omega_z'$  and in particular, for  $\eta = \eta'$ , it can be analytically estimated [52] as  $\kappa_U^{eff} = \kappa/2 - 2\eta^2(\gamma_\uparrow - \gamma_\downarrow)/[(\omega_z' - \Omega_U)^2 + \gamma_t^2/4]$ . By tuning  $\omega_z'$  close to  $\Omega_U$ , it is possible to obtain a negative effective decay rate ( $\kappa_U^{eff} < 0$ ) for  $\gamma_\uparrow > \gamma_\downarrow$ ; this gives rise to dynamical instabilities in the L1 and L2 regimes, which we can exploit to employ the spin ensemble  $\mathcal{T}$  as a frequency-dependent gain medium [7–9].

We now discuss the multi-stage dynamics [from A to D in Fig. 3(b)] associated with this mechanism. We initialise the system in the SR steady state of the Dicke model with photon losses ( $\lambda = 0.6$  and  $\kappa = 0.06$ ) and let it evolve with parameters characteristic of the L1 phase ( $\lambda = 0.2$ ,  $\gamma_\uparrow = 0.9$ ). Dynamics of the photon number are shown in Fig. 3(b). For the chosen parameters, the effective decay rate  $\kappa_L^{eff}$  ( $\kappa_U^{eff}$ ) is positive (negative), i.e., the upper polariton becomes unstable. Immediately after the quench (A), the photon field has sizeable overlap with the upper and lower polariton modes. Since in the initial SR steady state the boson is enslaved to matter,  $\langle a \rangle = -2\lambda/(\omega_c - i\kappa/2)\langle S^- \rangle$ , the amplitude of the lower mode is higher than the amplitude of the upper one. However, as the lower mode starts to decay and the upper one is enhanced, their amplitudes become comparable (B) and we observe beating at their two frequencies. At the stage C the photon number increases while the lower mode is largely suppressed. As a result, for long times (D) the oscillatory dynamics of the system is solely governed by  $\Omega_U$ . Such circumstance cannot occur in a more conventional driven-dissipative Dicke model [54], since in that case both upper and lower modes would be enhanced and survive at long times.

*Outlook.* A natural next step could consist in studying collective spin squeezing in the lasing regime [62–64], with the perspective of entanglement manipulation in spintronics platforms. This can be addressed, for instance, by simulating numerically exact dynamics at finite  $N$  [65, 66].

Recent studies have shown the usefulness of non-local dissipation in generating entanglement between distant qubits in both fields of quantum optics and spintronics, by investigating spins immersed in a optical cavity [67–69] and nitrogen-vacancy qubits in proximity to a magnetic medium [70]. For the latter, dynamical phase transitions in the magnet controlled by electrical pumping, may provide an efficient tunability of non-local dissipation, which could be studied along the lines of this work.

Finally, we did not include here the effect of short-range spin interactions breaking permutational symmetry. This is in general a challenging task since it requires a full many-body treatment of dynamics.

However, we expect that, deep inside the various phases, the dynamical phenomena discussed here will still hold in analogy with the character of other non-equilibrium phases in spin systems with competing short- and all-to-all interactions [71, 72].

*Acknowledgements.* JM and OC are indebted to P. Kirton for enlightening discussions. OC thanks S. Kelly and R. J. Valencia Tortora for helpful comments on this work. This project has been supported by the Deutsche Forschungsgemeinschaft (DFG, German Research Foundation) – Project-ID 429529648 – TRR 306 QuCoL-

iMa ("Quantum Cooperativity of Light and Matter"), by the Dynamics and Topology Centre funded by the State of Rhineland Palatinate, and in part by the National Science Foundation under Grant No. NSF PHY-1748958 (KITP program 'Non-Equilibrium Universality: From Classical to Quantum and Back'). A.L. acknowledges support by the Swiss National Science Foundation. S. Z. and Y. T. are supported by NSF under Grant No. DMR-1742928. I. C. acknowledges financial support from the H2020-FETFLAG-2018-2020 project "PhoQuS" (n.820392), and from the Provincia Autonoma di Trento.

---

[1] I. Carusotto and C. Ciuti, Quantum fluids of light, *Rev. Mod. Phys.* **85**, 299 (2013).

[2] H. Ritsch, P. Domokos, F. Brennecke, and T. Esslinger, Cold atoms in cavity-generated dynamical optical potentials, *Rev. Mod. Phys.* **85**, 553 (2013).

[3] A. A. Houck, H. E. Türeci, and J. Koch, On-chip quantum simulation with superconducting circuits, *Nat. Phys.* **8**, 292 (2012).

[4] A. Kirilyuk, A. V. Kimel, and T. Rasing, Ultrafast optical manipulation of magnetic order, *Rev. Mod. Phys.* **82**, 2731 (2010).

[5] G. La Rocca, Polariton lasing, *Nat. Photon.* **4**, 343 (2010).

[6] P. G. Savvidis, J. J. Baumberg, R. M. Stevenson, M. S. Skolnick, D. M. Whittaker, and J. S. Roberts, Angle-resonant stimulated polariton amplifier, *Phys. Rev. Lett.* **84**, 1547 (2000).

[7] T. Gao, C. Antón, T. C. H. Liew, M. Martín, Z. Hatzopoulos, L. Viña, P. Eldridge, and P. Savvidis, Spin selective filtering of polariton condensate flow, *Appl. Phys. Lett.* **107**, 011106 (2015).

[8] J. Lebreuilly, M. Wouters, and I. Carusotto, Towards strongly correlated photons in arrays of dissipative non-linear cavities under a frequency-dependent incoherent pumping, *Comptes Rendus Physique* **17**, 836 (2016).

[9] E. Kapit, M. Hafezi, and S. H. Simon, Induced self-stabilization in fractional quantum Hall states of light, *Phys. Rev. X* **4**, 031039 (2014).

[10] J. J. Hauser, Magnetic proximity effect, *Phys. Rev.* **187**, 580 (1969).

[11] E. Saitoh, M. Ueda, H. Miyajima, and G. Tatara, Conversion of spin current into charge current at room temperature: Inverse spin-Hall effect, *Appl. Phys. Lett.* **88**, 182509 (2006).

[12] K. Uchida, J. Xiao, H. Adachi, J. Ohe, S. Takahashi, J. Ieda, T. Ota, Y. Kajiwara, H. Umezawa, H. Kawai, G. E. Bauer, S. Maekawa, and E. Saitoh, Spin Seebeck insulator, *Nat. Mater.* **9**, 894 (2010).

[13] Y. Kajiwara, K. Harii, S. Takahashi, J. Ohe, K. Uchida, M. Mizuguchi, H. Umezawa, H. Kawai, K. Ando, K. Takanashi, *et al.*, Transmission of electrical signals by spin-wave interconversion in a magnetic insulator, *Nature* **464**, 262 (2010).

[14] F. D. Czeschka, L. Dreher, M. S. Brandt, M. Weiler, M. Althammer, I. M. Imort, G. Reiss, A. Thomas, W. Schoch, W. Limmer, H. Huebl, R. Gross, and S. T. Goennenwein, Scaling behavior of the spin pumping effect in ferromagnet–platinum bilayers, *Phys. Rev. Lett.* **107** (2011).

[15] S. Y. Huang, X. Fan, D. Qu, Y. P. Chen, W. G. Wang, J. Wu, T. Y. Chen, J. Q. Xiao, and C. L. Chien, Transport magnetic proximity effects in platinum, *Phys. Rev. Lett.* **109**, 107204 (2012).

[16] M. Althammer, S. Meyer, H. Nakayama, M. Schreier, S. Altmannshofer, M. Weiler, H. Huebl, S. Geprägs, M. Opel, R. Gross, D. Meier, C. Klewe, T. Kuschel, J.-M. Schmalhorst, G. Reiss, L. Shen, A. Gupta, Y.-T. Chen, G. E. W. Bauer, E. Saitoh, and S. T. B. Goennenwein, Quantitative study of the spin Hall magnetoresistance in ferromagnetic insulator/normal metal hybrids, *Phys. Rev. B* **87**, 224401 (2013).

[17] T. Lin, C. Tang, and J. Shi, Induced magneto-transport properties at palladium/yttrium iron garnet interface, *Appl. Phys. Lett.* **103**, 132407 (2013).

[18] C. Hahn, G. de Loubens, O. Klein, M. Viret, V. V. Naletov, and J. Ben Youssef, Comparative measurements of inverse spin Hall effects and magnetoresistance in YIG/Pt and YIG/Ta, *Phys. Rev. B* **87**, 174417 (2013).

[19] C. Kittel and C. Y. Fong, *Quantum theory of solids*, Vol. 5 (Wiley New York, 1963).

[20] M. I. Dyakonov and V. Perel, Current-induced spin orientation of electrons in semiconductors, *Phys. Lett. A* **35**, 459 (1971).

[21] S. O. Demokritov, V. E. Demidov, O. Dzyapko, G. A. Melkov, A. A. Serga, B. Hillebrands, and A. N. Slavin, Bose–Einstein condensation of quasi-equilibrium magnons at room temperature under pumping, *Nature* **443**, 430 (2006).

[22] V. E. Demidov, O. Dzyapko, S. O. Demokritov, G. A. Melkov, and A. N. Slavin, Observation of spontaneous coherence in Bose–Einstein condensate of magnons, *Phys. Rev. Lett.* **100**, 047205 (2008).

[23] R. A. Duine, A. Brataas, S. A. Bender, and Y. Tserkovnyak, Spintronics and magnon Bose–Einstein condensation, in *Universal Themes of Bose–Einstein Condensation*, edited by N. P. Proukakis, D. W. Snoke, and P. B. Littlewood (Cambridge University Press, 2017) p. 505–524.

[24] T. Giamarchi, C. Rüegg, and O. Tchernyshyov, Bose–Einstein condensation in magnetic insulators, *Nat. Phys.* **4**, 198 (2008).

[25] L. Berger, Emission of spin waves by a magnetic mul-

tilayer traversed by a current, Phys. Rev. B **54**, 9353 (1996).

[26] Y. M. Bunkov and G. E. Volovik, Magnon condensation into a  $Q$  ball in  ${}^3\text{He}-B$ , Phys. Rev. Lett. **98**, 265302 (2007).

[27] Y. M. Bunkov and G. E. Volovik, Bose–Einstein condensation of magnons in superfluid  ${}^3\text{He}$ , Low Temp. Phys. **150**, 135 (2008).

[28] S. A. Bender, R. A. Duine, and Y. Tserkovnyak, Electronic pumping of quasiequilibrium Bose–Einstein-condensed magnons, Phys. Rev. Lett. **108**, 246601 (2012).

[29] S. A. Bender, R. A. Duine, A. Brataas, and Y. Tserkovnyak, Dynamic phase diagram of dc-pumped magnon condensates, Phys. Rev. B **90**, 094409 (2014).

[30] E. L. Fjærbu, N. Rohling, and A. Brataas, Electrically driven Bose–Einstein condensation of magnons in antiferromagnets, Phys. Rev. B **95**, 144408 (2017).

[31] S. Takei, Spin transport in an electrically driven magnon gas near Bose–Einstein condensation: Hartree–Fock–Keldysh theory, Phys. Rev. B **100**, 134440 (2019).

[32] T. Wimmer, M. Althammer, L. Liensberger, N. Vlietstra, S. Geprägs, M. Weiler, R. Gross, and H. Huebl, Spin transport in a magnetic insulator with zero effective damping, Phys. Rev. Lett. **123**, 257201 (2019).

[33] C. Hurd, *The Hall effect in metals and alloys* (Springer Science & Business Media, 2012).

[34] J. E. Hirsch, Spin Hall effect, Phys. Rev. Lett. **83**, 1834 (1999).

[35] Y. K. Kato, R. C. Myers, A. C. Gossard, and D. D. Awschalom, Observation of the spin Hall effect in semiconductors, Science **306**, 1910 (2004).

[36] V. Sih, R. Myers, Y. Kato, W. Lau, A. Gossard, and D. Awschalom, Spatial imaging of the spin Hall effect and current-induced polarization in two-dimensional electron gases, Nat. Phys. **1**, 31 (2005).

[37] J. Wunderlich, B. Kaestner, J. Sinova, and T. Jungwirth, Experimental observation of the spin–Hall effect in a two-dimensional spin–orbit coupled semiconductor system, Phys. Rev. Lett. **94**, 047204 (2005).

[38] S. O. Valenzuela and M. Tinkham, Direct electronic measurement of the spin Hall effect, Nature **442**, 176 (2006).

[39] J. C. Slonczewski, Current-driven excitation of magnetic multilayers, J. Magn. Magn. Mater. **159**, L1 (1996).

[40] D. C. Ralph and M. D. Stiles, Spin transfer torques, J. Magn. Magn. Mater. **320**, 1190 (2008).

[41] Y. Tserkovnyak and S. A. Bender, Spin Hall phenomenology of magnetic dynamics, Phys. Rev. B **90**, 014428 (2014).

[42] B. Flebus, S. A. Bender, Y. Tserkovnyak, and R. A. Duine, Two-fluid theory for spin superfluidity in magnetic insulators, Phys. Rev. Lett. **116**, 117201 (2016).

[43] P. Kirton, M. M. Roses, J. Keeling, and E. G. Dalla Torre, Introduction to the Dicke model: From equilibrium to nonequilibrium, and vice versa, Advanced Quantum Technologies **2**, 1800043 (2019).

[44] C. Emary and T. Brandes, Chaos and the quantum phase transition in the Dicke model, Phys. Rev. E **67**, 066203 (2003).

[45] M. Bhaseen, J. Mayoh, B. Simons, and J. Keeling, Dynamics of nonequilibrium Dicke models, Phys. Rev. A **85**, 013817 (2012).

[46] J. Keeling, M. Bhaseen, and B. Simons, Collective dynamics of Bose–Einstein condensates in optical cavities, Phys. Rev. Lett. **105**, 043001 (2010).

[47] F. Reiter, T. L. Nguyen, J. P. Home, and S. F. Yelin, Cooperative breakdown of the oscillator blockade in the Dicke model, Phys. Rev. Lett. **125**, 233602 (2020).

[48] H. P. Breuer, F. Petruccione, *et al.*, *The theory of open quantum systems* (Oxford University Press on Demand, 2002).

[49] I. D. Mayergoyz, G. Bertotti, and C. Serpico, *Nonlinear magnetization dynamics in nanosystems* (Elsevier, 2009).

[50] T. L. Gilbert, A phenomenological theory of damping in ferromagnetic materials, IEEE Trans. Magn. **40**, 3443 (2004).

[51] N. Bode, S. V. Kusminskiy, R. Egger, and F. von Oppen, Scattering theory of current-induced forces in mesoscopic systems, Phys. Rev. Lett. **107**, 036804 (2011).

[52] See Supplemental Material for MF equations of motion, Gilbert damping, lasing instabilities, polariton analysis and cumulants expansion.

[53] R. H. Dicke, Coherence in spontaneous radiation processes, Phys. Rev. **93**, 99 (1954).

[54] P. Kirton and J. Keeling, Superradiant and lasing states in driven–dissipative Dicke models, New J. Phys. **20**, 015009 (2018).

[55] P. Kirton and J. Keeling, Suppressing and restoring the Dicke superradiance transition by dephasing and decay, Phys. Rev. Lett. **118**, 123602 (2017).

[56] D. Tieri, M. Xu, D. Meiser, J. Cooper, and M. Holland, Theory of the crossover from lasing to steady state superradiance, arXiv preprint arXiv:1702.04830 (2017).

[57] W. Kopylov, M. Radonjić, T. Brandes, A. Balaž, and A. Pelster, Dissipative two-mode Tavis–Cummings model with time-delayed feedback control, Phys. Rev. A **92**, 063832 (2015).

[58] E. G. Dalla Torre, S. Diehl, M. D. Lukin, S. Sachdev, and P. Strack, Keldysh approach for nonequilibrium phase transitions in quantum optics: Beyond the Dicke model in optical cavities, Phys. Rev. A **87**, 023831 (2013).

[59] J. Lang and F. Piazza, Critical relaxation with over-damped quasiparticles in open quantum systems, Phys. Rev. A **94**, 033628 (2016).

[60] A. A. Serga, C. W. Sandweg, V. I. Vasyuchka, M. B. Jungfleisch, B. Hillebrands, A. Kreisel, P. Kopietz, and M. P. Kostylev, Brillouin light scattering spectroscopy of parametrically excited dipole–exchange magnons, Phys. Rev. B **86**, 134403 (2012).

[61] Y. Tserkovnyak, A. Brataas, and G. E. W. Bauer, Enhanced Gilbert damping in thin ferromagnetic films, Phys. Rev. Lett. **88**, 117601 (2002).

[62] J. Ma, X. Wang, C. P. Sun, and F. Nori, Quantum spin squeezing, Phys. Rep. **509**, 89 (2011).

[63] L. Pezze, A. Smerzi, M. K. Oberthaler, R. Schmied, and P. Treutlein, Quantum metrology with nonclassical states of atomic ensembles, Rev. Mod. Phys. **90**, 035005 (2018).

[64] M. Koppenhöfer, P. Groszkowski, H. K. Lau, and A. A. Clerk, Dissipative superradiant spin amplifier for enhanced quantum sensing (2021), arXiv:2111.15647 [quant-ph].

[65] N. Shammah, S. Ahmed, N. Lambert, S. De Liberato, and F. Nori, Open quantum systems with local and collective incoherent processes: Efficient numerical simulations using permutational invariance, Phys. Rev. A **98**, 063815 (2018).

[66] A. Lerose and S. Pappalardi, Bridging entanglement dynamics and chaos in semiclassical systems, Phys. Rev. A

**102**, 032404 (2020).

[67] K. Seetharam, A. Lerose, R. Fazio, and J. Marino, Correlation engineering via non-local dissipation, arXiv:2101.06445 (2021).

[68] K. Seetharam, A. Lerose, R. Fazio, and J. Marino, Dynamical scaling of correlations generated by short- and long-range dissipation (2021), arXiv:2110.09547 [cond-mat.quant-gas].

[69] J. Marino, Universality class of Ising critical states with long-range losses (2021), arXiv:2108.12422 [cond-mat.stat-mech].

[70] J. Zou, S. Zhang, and Y. Tserkovnyak, Bell-state generation for spin qubits via dissipative coupling, arXiv:2108.07365 (2021).

[71] A. Lerose, B. Žunkovič, J. Marino, A. Gambassi, and A. Silva, Impact of nonequilibrium fluctuations on prethermal dynamical phase transitions in long-range interacting spin chains, Phys. Rev. B **99**, 045128 (2019).

[72] B. Zhu, J. Marino, N. Y. Yao, M. D. Lukin, and E. A. Demler, Dicke time crystals in driven-dissipative quantum many-body systems, New J. Phys. **21**, 073028 (2019).

[73] L. Landau and E. Lifshitz, On the theory of the dispersion of magnetic permeability in ferromagnetic bodies, in *Perspectives in Theoretical Physics* (Elsevier, 1992) pp. 51–65.

[74] T. Gilbert, A lagrangian formulation of the gyromagnetic equation of the magnetization field, Phys. Rev. **100**, 1243 (1955).

[75] T. Holstein and H. Primakoff, Field dependence of the intrinsic domain magnetization of a ferromagnet, Phys. Rev. **58**, 1098 (1940).

[76] G. S. Agarwal, R. R. Puri, and R. P. Singh, Atomic Schrödinger cat states, Phys. Rev. A **56**, 2249 (1997).

[77] M. Xu, *Theory of steady-state superradiance*, Ph.D. thesis, University of Colorado at Boulder (2016).

[78] M. A. Norcia, R. J. Lewis-Swan, J. R. Cline, B. Zhu, A. M. Rey, and J. K. Thompson, Cavity-mediated collective spin-exchange interactions in a strontium superradiant laser, Science **361**, 259 (2018).

[79] H. Haken, Cooperative phenomena in systems far from thermal equilibrium and in nonphysical systems, Rev. Mod. Phys. **47**, 67 (1975).

[80] H. Haken, The semiclassical approach and its applications, in *Laser Theory* (Springer, 1984) pp. 173–248.

[81] J. W. Negele and H. Orland, *Quantum many-particle systems* (CRC Press, 2018).

[82] K. Huang, *Introduction to statistical physics* (Chapman and Hall/CRC, 2009).

[83] M. Lewenstein and L. You, Quantum phase diffusion of a Bose–Einstein condensate, Phys. Rev. Lett. **77**, 3489 (1996).

[84] I. Amelio and I. Carusotto, Theory of the coherence of topological lasers, Phys. Rev. X **10**, 041060 (2020).

## Supplemental Material:

### Competition between lasing and superradiance under spintronic pumping

Oksana Chelpanova<sup>1</sup>, Alessio Leroose<sup>2</sup>, Shu Zhang<sup>3,4</sup>, Iacopo Carusotto<sup>5</sup>, Yaroslav Tserkovnyak<sup>4</sup>, Jamir Marino<sup>1,6</sup>

<sup>1</sup>*Institut für Physik, Johannes Gutenberg Universität Mainz, D-55099 Mainz, Germany*

<sup>2</sup>*Department of Theoretical Physics, University of Geneva, Quai Ernest-Ansermet 30, 1205 Geneva, Switzerland*

<sup>3</sup>*Max-Planck-Institut für Physik komplexer Systeme, 01187 Dresden, Germany*

<sup>4</sup>*Department of Physics and Astronomy, University of California, Los Angeles, CA 90095, USA*

<sup>5</sup>*INO-CNR BEC Center and Dipartimento di Fisica, Università di Trento, 38123 Trento, Italy*

<sup>6</sup>*Kavli Institute for Theoretical Physics, University of California, Santa Barbara, CA 93106-4030, USA*

### Appendix A: Stability analysis

The mean-field equations of motion used to derive the phase diagram in Fig. 2(a) read

$$\begin{cases} \frac{d\langle a \rangle}{dt} = -i\eta\langle\mathcal{T}^-\rangle - (i\omega_c + \kappa/2)\langle a \rangle - i\lambda(\langle\mathcal{S}^+ \rangle + \langle\mathcal{S}^- \rangle) \\ \frac{d\langle\mathcal{S}^z \rangle}{dt} = i\lambda(\langle a \rangle + \langle a^\dagger \rangle)(\langle\mathcal{S}^- \rangle - \langle\mathcal{S}^+ \rangle) + i\eta'(\langle\mathcal{T}^+ \rangle\langle\mathcal{S}^- \rangle - \langle\mathcal{T}^- \rangle\langle\mathcal{S}^+ \rangle) \\ \frac{d\langle\mathcal{S}^- \rangle}{dt} = -i\omega_z\langle\mathcal{S}^- \rangle + 2i\lambda(\langle a \rangle + \langle a^\dagger \rangle)\langle\mathcal{S}^z \rangle + 2i\eta'\langle\mathcal{T}^- \rangle\langle\mathcal{S}^z \rangle \\ \frac{d\langle\mathcal{T}^z \rangle}{dt} = i\eta(\langle a^\dagger \rangle\langle\mathcal{T}^- \rangle - \langle a \rangle\langle\mathcal{T}^+ \rangle) - i\eta'(\langle\mathcal{T}^+ \rangle\langle\mathcal{S}^- \rangle - \langle\mathcal{T}^- \rangle\langle\mathcal{S}^+ \rangle) + \frac{\gamma_\uparrow - \gamma_\downarrow}{2} - \gamma_t\langle\mathcal{T}^z \rangle \\ \frac{d\langle\mathcal{T}^- \rangle}{dt} = -(i\omega_z' + \gamma_t/2)\langle\mathcal{T}^- \rangle + 2i\eta\langle a \rangle\langle\mathcal{T}^z \rangle + 2i\eta'\langle\mathcal{T}^z \rangle\langle\mathcal{S}^- \rangle. \end{cases} \quad (\text{A1})$$

Here we neglected higher order correlations which are all suppressed as  $1/N$ , approximating  $\langle AB \rangle \approx \langle A \rangle \langle B \rangle$ . This approximation is exact in the  $N \rightarrow \infty$  limit [43]. All variables in Eq. A1 are intensive, since they are normalized in such a way that they are independent of the number of spins  $N$  as  $N \rightarrow \infty$ .

From Eqs. (A1) we study the instabilities of the normal state (NS). By perturbing with small fluctuations around the normal state expectation values  $\langle a \rangle = \langle a \rangle_0 + \delta a$ ,  $\langle \mathcal{S}^- \rangle = \langle \mathcal{S}^- \rangle_0 + \delta \mathcal{S}^-$ ,  $\langle \mathcal{T}^- \rangle = \langle \mathcal{T}^- \rangle_0 + \delta \mathcal{T}^-$ , (with  $\langle a \rangle_0 = \langle \mathcal{S}^- \rangle_0 = \langle \mathcal{T}^- \rangle_0 = 0$  and  $\langle \mathcal{S}^z \rangle = -1/2$  and  $\langle \mathcal{T}^z \rangle = (\gamma_\uparrow - \gamma_\downarrow)/2\gamma_t$ ), we can find a linear system of equations for these deviations from the NS, which can be written in the form  $\dot{x} = Ax$ , where  $x = (\delta a, \delta a^*, \delta \mathcal{S}^-, \delta \mathcal{S}^+, \delta \mathcal{T}^-, \delta \mathcal{T}^+)^T$ . This matrix reads

$$A = \begin{bmatrix} -i\omega_c - \frac{\kappa}{2} & 0 & -i\lambda & -i\lambda & -i\eta & 0 \\ 0 & i\omega_c - \frac{\kappa}{2} & i\lambda & i\lambda & 0 & i\eta \\ -i\lambda & -i\lambda & -i\omega_z & 0 & -i\eta' & 0 \\ i\lambda & i\lambda & 0 & i\omega_z & 0 & i\eta' \\ 2i\eta\langle\mathcal{T}^z \rangle & 0 & 2i\eta'\langle\mathcal{T}^z \rangle & 0 & -i\omega_z' - \frac{\gamma_t}{2} & 0 \\ 0 & -2i\eta\langle\mathcal{T}^z \rangle & 0 & -2i\eta'\langle\mathcal{T}^z \rangle & 0 & i\omega_z' - \frac{\gamma_t}{2} \end{bmatrix}. \quad (\text{A2})$$

By performing a stability analysis [54], one can distinguish the set of parameters for which the normal state is stable. Results are shown in Fig. 4. The white region with all negative eigenvalues corresponds to the stable normal phase. The purple region with one real positive eigenvalue matches the boundary of SR phase in Fig. 2(a). The yellow region with two positive complex conjugate eigenvalues corresponds to lasing. The parameters in the orange region corresponds to the three positive eigenvalues of the matrix (A2). The boundary between the SR and NS is well approximated by the  $\lambda_c$  of the Dicke model [44, 54]. However, this simple stability analysis does not capture the difference between dynamical phases such as L1, L2 and IR in Fig. 2 (a) of the main text, which require a through evaluation of the far-from-equilibrium dynamics encoded in Eqs. (A1).

When we pump the system at a frequency resonant with the upper polaritonic frequency  $\Omega_U$ , the boundary of the lasing region can undergo drastic changes. As it is shown in Fig. 5, the boundary between normal state and lasing phase is now solely defined by the critical value of pumping rate  $\gamma_\uparrow/\gamma_t$ , and does not depend on  $\lambda$ .

### Appendix B: Gilbert damping

For the magnon condensate mode, dissipation in the form of Gilbert damping slows down the spontaneous precession of the magnetic order parameter like a viscous drag [40]. It is particularly suitable in the weak-damping scenario to describe the relaxation of the precessional motion back to the equilibrium state (in the absence of external pumping) along a spiral trajectory without losing coherence. The semiclassical Landau-Lifshitz-Gilbert equation [50, 73, 74] of a spin  $\mathbf{s}$  reads  $d\mathbf{s}/dt = \mathbf{s} \times \mathbf{h}_{\text{eff}} - \alpha_G \mathbf{s} \times d\mathbf{s}/dt$ , where  $\mathbf{h}_{\text{eff}}$  is an effective Zeeman field fixing the equilibrium spin orientation, and  $\alpha_G$  is the Gilbert damping. A small-angle spin precession can be mapped to the motion of a harmonic oscillator

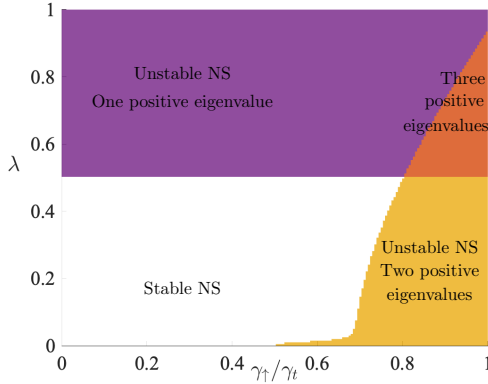


FIG. 4. Stability analysis of the normal state. The parameters are the same as in Fig. 2(a). The normal state is indicated in white color. The purple color corresponds to one real positive eigenvalue of the matrix  $A$  and it indicates superradiance. The yellow region corresponds to two complex conjugated eigenvalues with positive real part and it corresponds to the lasing region. The orange region corresponds to the three positive eigenvalues. Here  $\omega = \omega'_z$ .

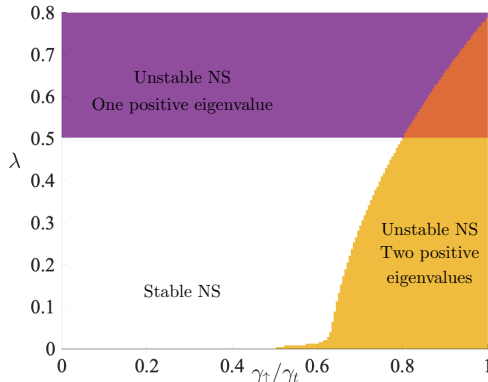


FIG. 6. Stability analysis for model with Gilbert damping. All parameters are as in Fig. 2(a),  $\kappa = 0.04$ , and the color code follows Fig. 4.

with creation and annihilation operators [75]  $a^\dagger$  and  $a$ , where  $s_z = s - a^\dagger a \approx s$  with  $\mathcal{S}$  being the spin length. The Landau-Lifshitz-Gilbert equation in the lowest order thus becomes  $(1 + i\kappa\alpha_G)d\langle a \rangle/dt = -i\omega_c\langle a \rangle$ , where  $\omega_c = |\mathbf{h}_{\text{eff}}|$ . Such a form of the viscous drag can also be derived by coupling the bosonic mode  $a$  to an Ohmic bath and eliminating the bath degrees of freedom following a standard Caldeira-Leggett derivation [48].

For our model (1), the Gilbert damping modifies the mean field equation of motion for the expectation value of the bosonic mode into

$$(1 + i\kappa/2) \frac{d\langle a \rangle}{dt} = -i(\omega_c - \tilde{\Delta})\langle a \rangle - i\eta\langle \mathcal{T}^- \rangle - i\lambda(\langle \mathcal{S}^+ \rangle + \langle \mathcal{S}^- \rangle) + \frac{B(t)}{\sqrt{N}}. \quad (\text{B1})$$

Here  $\tilde{\Delta}$  is a Lamb shift and  $B(t)$  is the noise term that results from the bath [48]. This term is suppressed as  $1/\sqrt{N}$  for large  $N$ , therefore vanishing in the mean field limit. The dynamical phase diagram with this type of dissipation is plotted in Fig. 7. Here we fixed  $\tilde{\omega}_c = \omega_c - \tilde{\Delta} = 1$  and  $\kappa = 0.04$ . Qualitatively, the diagram remains the same as if we used photon losses; we still recognize five different dynamical responses as superradiance (SR), normal state (NS), and lasing and SR persistent oscillations (L1 and L2), as well as irregular dynamics (IR), although the boundaries between phases are quantitatively modified. Results are in a good agreement with predictions obtained from the

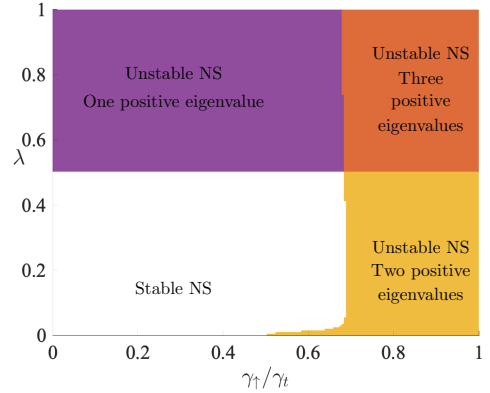


FIG. 5. Stability analysis with the resonance condition  $\omega'_z = \Omega_U$ . The rest of parameters are as in Fig. 2(a). The vertical boundary between normal state (white) and lasing (yellow) is given by the critical pumping rate  $\gamma_{\uparrow c} = 0.6875$  (see Eq. E2).

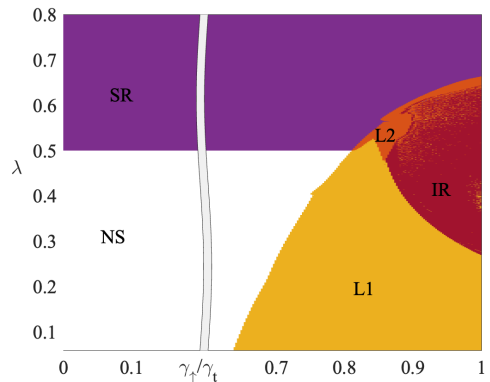


FIG. 7. Dynamical phase diagram with Gilbert damping (see Eqn. B1). All parameters are as in Fig. 6 and the color code follows Fig. 2(a).

stability analysis (cf. with Fig. 6).

### Appendix C: Lasing in the Tavis-Cummings model

We consider the limit  $\lambda = \eta' = 0$ . The system in this case is endowed with a U(1) symmetry [43], corresponding to conservation of total number of excitations (spins+boson); non-trivial solutions of the mean-field equations of motion A1 that break dynamically the symmetry can be expressed in the form (see for instance Refs.[56, 57])

$$\langle a \rangle \rightarrow a_0 e^{-i\Delta t}, \quad \langle \mathcal{T}^\pm \rangle \rightarrow \mathcal{T}_0^\pm e^{\pm i\Delta t} \quad (C1)$$

where  $\Delta$  is a characteristic frequency to be self-consistently determined. Substituting (C1) into Eqs. (A1) one obtains:

$$\begin{cases} \Delta = \frac{\kappa\omega'_z + \gamma_t\omega_c}{\kappa + \gamma_t} \\ \langle \mathcal{T}^z \rangle = \frac{\gamma_t\kappa}{2\eta^2} \left( \frac{(\omega_c - \omega'_z)^2}{(\kappa + \gamma_t)^2} + \frac{1}{4} \right) \\ \mathcal{T}_0^\pm = \sqrt{\frac{\gamma_t\tau_0^z\kappa}{\eta^2} \left( \frac{(\omega_c - \omega'_z)^2}{(\kappa + \gamma_t)^2} + \frac{1}{4} \right) - \frac{\gamma_t^2\kappa^2}{2\eta^4} \left( \frac{(\omega_c - \omega'_z)^2}{(\kappa + \gamma_t)^2} + \frac{1}{4} \right)^2}. \end{cases} \quad (C2)$$

Here  $\tau_0^z = (\gamma_\uparrow - \gamma_\downarrow)/2\gamma_t$  is the steady state value of the magnetization in the pumped subsystem. In the  $\omega_c \approx \omega'_z \equiv \omega$  limit one can further simplify these expressions to acquire physical insight:

$$\begin{cases} \Delta = \omega \\ \langle \mathcal{T}^z \rangle = \frac{\gamma_t\kappa}{8\eta^2} \\ \langle \mathcal{T}^\pm \rangle = \left( \sqrt{\frac{\gamma_t\tau_0^z\kappa}{4\eta^2} - \frac{\gamma_t^2\kappa^2}{32\eta^4}} \right) e^{\pm i\omega t} \\ n = \frac{\gamma_t}{\kappa} (\tau_0^z - \langle \mathcal{T}^z \rangle) \end{cases} \quad (C3)$$

The lasing solution exists only if the expression under square root is positive. This condition is satisfied when the photon loss rate  $\kappa < \kappa_c = 4\eta^2/\gamma_t$ . By introducing photon losses in the form of Gilbert damping (B1) and repeating similar calculations, we find

$$\frac{2\eta^2\tau_0^z}{\gamma_t} - \kappa/4 + O(\eta^4) \geq 0.$$

which gives the same critical value of  $\kappa_c$ .

### Appendix D: Instabilities from adiabatic elimination

We now work out analytically some dynamical properties of our system in the limit of a fast relaxing bath [76], known as adiabatic elimination of the bath in quantum optics. We choose  $\gamma_t$  large enough compared to  $\eta$  and  $\eta'$  to induce relaxation of the incoherent subsystem  $\mathcal{T}$  much faster than the dynamics of the coherent one  $\mathcal{S}$ . Following Refs. [77, 78], we can enslave the spins of the incoherent ensembles to those of the Dicke system, by setting the time derivatives of the former to zero:

$$\begin{cases} \langle \mathcal{T}^- \rangle \simeq \frac{2\langle \mathcal{T}^z \rangle(\omega'_z + i\gamma_t/2)}{\omega'^2_z + \gamma_t^2/4} (\eta\langle a \rangle + \eta'\langle \mathcal{S}^- \rangle) + \dots, \\ \langle \mathcal{T}^+ \rangle \simeq \frac{2\langle \mathcal{T}^z \rangle(\omega'_z - i\gamma_t/2)}{\omega'^2_z + \gamma_t^2/4} (\eta\langle a^\dagger \rangle + \eta'\langle \mathcal{S}^+ \rangle) + \dots \\ \langle \mathcal{T}^z \rangle \simeq (\gamma_\uparrow - \gamma_\downarrow)/2\gamma_t + \dots, \end{cases} \quad (D1)$$

where we neglect terms in higher orders of  $1/\gamma_t$ . This is equivalent to assuming that spins in the  $\mathcal{T}$  ensemble have already reached their steady state. When substituting Eq. (D1) into the equations of motion for the normalized cavity mode and for the spins of the coherent subsystem  $\mathcal{S}$ , we find

$$\langle \dot{a} \rangle = -\left(i\omega_c + \frac{\kappa}{2}\right)\langle a \rangle - i\eta \left( \frac{2\eta\langle \mathcal{T}^z \rangle}{(\omega'_z - \frac{i\gamma_t}{2})} \langle a \rangle + \frac{2\eta'\langle \mathcal{T}^z \rangle}{(\omega'_z - \frac{i\gamma_t}{2})} \langle \mathcal{S}^- \rangle \right) - i\lambda (\langle \mathcal{S}^+ \rangle + \langle \mathcal{S}^- \rangle). \quad (D2)$$

The dissipative dynamics of the subsystem  $\mathcal{S}$  and the photon mode can now be described with Lindblad terms with effective jump operators  $L_1 = \sqrt{\gamma_\uparrow} \tau_i^+$  and  $L_2 = \sqrt{\gamma_\downarrow} \tau_i^-$ , given in terms of  $a$  and  $\mathcal{S}^-$  through Eqs. (D1). From Eq. (D2), we find

$$\langle \dot{a} \rangle = (-i\tilde{\omega} - \tilde{\kappa}) \langle a \rangle - i\lambda (\langle \mathcal{S}^+ \rangle + \langle \mathcal{S}^- \rangle) - \frac{2i\eta\eta' \langle \mathcal{T}^z \rangle}{(\omega'_z - \frac{i\gamma_t}{2})} \langle \mathcal{S}^- \rangle, \quad (\text{D3})$$

where

$$\tilde{\omega} = \omega_c - \frac{2\eta^2 \omega'_z \langle \mathcal{T}^z \rangle}{\left(\omega'^2_z + \frac{\gamma_t^2}{4}\right)}, \quad \tilde{\kappa} = \frac{\kappa}{2} - \frac{\gamma_\uparrow - \gamma_\downarrow}{2} \frac{\eta^2}{\omega'^2_z + \gamma_t^2/4}. \quad (\text{D4})$$

According to the second of the formulas in Eq. (D4), when the incoherent ensemble is in the population inverted state, the photon mode becomes effectively pumped due to the weak interaction with  $\mathcal{T}$ . If this pumping overcomes the photon decay  $\kappa$ , the photon number starts to grow and dynamical instabilities are triggered.

The equation that effectively governs the dynamics of the coherent subsystem can be derived in the same way and reads

$$\langle \dot{\mathcal{S}}^- \rangle = -i\omega_z \langle \mathcal{S}^- \rangle + 2i\lambda (\langle a \rangle + \langle a^\dagger \rangle) \langle \mathcal{S}^z \rangle + \frac{2i\eta'(\omega'_z + i\gamma_t/2)(\gamma_\uparrow - \gamma_\downarrow) \langle \mathcal{S}^z \rangle}{\gamma_t(\omega'^2_z + \gamma_t^2/4)} (\eta \langle a \rangle + \eta' \langle \mathcal{S}^- \rangle).$$

Here the effective contribution from the dissipator has the form

$$\langle \dot{\mathcal{S}}^- \rangle \propto \frac{\eta'(\gamma_\uparrow - \gamma_\downarrow)(-\langle \mathcal{S}^z \rangle)}{(\omega'^2_z + \gamma_t^2/4)} (\eta \langle a \rangle + \eta' \langle \mathcal{S}^- \rangle).$$

Therefore, for regions with  $\gamma_\uparrow > \gamma_\downarrow$ , spins in the system are effectively pumped by a rate proportional to the magnetization along  $\hat{z}$ , provided  $\langle S_z \rangle$  is negative (as it occurs in the NS or in the SR phase).

Adiabatic elimination of the incoherent subsystem gives correct predictions for  $\lambda = 0$ . For  $\lambda \neq 0$ , light and matter hybridize and a separate analysis is required; we elaborate on this in the next subsection.

### Appendix E: Polaritons in the dynamics of L1

Frequencies of the polaritons can be evaluated by expanding the Dicke model in a leading order Holstein-Primakoff approximation and by diagonalizing the resulting hamiltonian [44]

$$\Omega_{U/L} = \sqrt{\left(\omega_c^2 + \omega_z^2 \pm \sqrt{(\omega_c^2 - \omega_z^2)^2 + 16\lambda^2 \omega_z \omega_c}\right)}/2. \quad (\text{E1})$$

For the parameters of Fig. 2 the upper polaritonic frequency is  $\Omega_U = 1.63$  and the lower one is  $\Omega_L = 0.63$ . Since the photon amplitude operator  $a$  can be written as the sum of upper and lower polaritons, both modes contribute to the dynamics of  $n$ . However, their effective decay rates are different, giving rise to different short- and long-time behavior of the the dynamics of  $n$ . Inside the SR phase the difference between the amplitudes of upper and lower modes can be estimated using the Holstein-Primakoff analysis [44] as

$$\frac{|\psi_U|}{|\psi_L|} = \left| \frac{1 - 2\lambda(\omega_c + i\kappa/2) / (\omega_c^2 + \kappa^2/4)}{1 + 2\lambda(\omega_c + i\kappa/2) / (\omega_c^2 + \kappa^2/4)} \right| \approx \left| \frac{1 - 2\lambda/\omega_c}{1 + 2\lambda/\omega_c} \right|$$

which is much more smaller than 1 close to the  $\lambda_c$ . If we prepare an initial state inside SR phase and let it evolve with parameters that correspond to any oscillatory phase (L1, L2, IR), the short-time dynamics is mostly governed by the lower polariton, as its amplitude dominates.

We now provide estimates for the effective damping of the photon mode in various system's parameters regimes, which is given by  $n \propto \exp(-\kappa_{\text{eff}} t)$ , ignoring oscillations. Depending on the level splitting of the  $\mathcal{T}$  spins,  $\omega'_z$ ,  $\kappa_{\text{eff}}$  can be varied. Fig. 8 shows the effective damping  $\kappa_{\text{eff}}$  of the photonic modes as function of  $\omega'_z$ . The effective damping coefficients  $\kappa_{U/L}^{\text{eff}}$  of lower and upper mode are extracted from dynamics of  $n$  at short and long timescales, respectively. As one can see from Fig. 8, both damping coefficients have a minimum close to the resonance upper

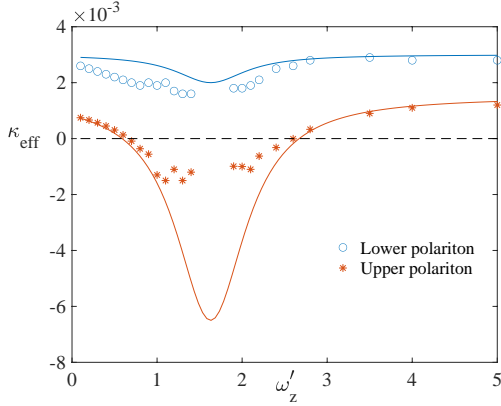


FIG. 8. Effective damping  $\kappa_{\text{eff}}$  of the photonic mode extracted in the stage C of dynamics in Fig. 3 in the main text, as a function of the frequency of the incoherent subsystem. Close to the resonant frequency of the upper polariton,  $\Omega_U = 1.63$ , the effective damping  $\kappa_U^{\text{eff}}$  can change sign, indicating a dynamical instability, which results into the polariton lasing shown in Fig. 3.

polariton frequency. Also, for all frequencies  $\omega'_z$ , the damping of the lower mode is faster than the upper polariton, which is the reason why we observe oscillations at long times with frequency  $\Omega_U$  only. The upper mode is more long-lived and can even be enhanced via pumping, when  $\omega'_z$  is close enough to the upper polaritonic frequency  $\Omega_U$ , resulting in lasing. For  $\eta = \eta'$ , the effective damping of the upper polariton mode can be analytically estimated as  $\kappa_U^{\text{eff}} = \kappa/2 - 2\eta^2(\gamma_{\uparrow} - \gamma_{\downarrow}) / [(\omega'_z - \Omega_U)^2 + \gamma_t^2/4]$  (solid red line in Fig. 8).

If the system is pumped resonantly with the upper polariton frequency  $\omega'_z \simeq \Omega_U$ , the critical value of  $\gamma_{\uparrow}$  at which the lasing region occurs can be estimated as

$$\frac{\gamma_{\uparrow}}{\gamma_t} \geq \frac{1}{2} \left( \frac{\kappa \gamma_t}{16\eta^2} + 1 \right), \quad (\text{E2})$$

following a calculation similar to the one leading to Eq. (D4). In this case, lasing is obtained at a pumping frequency smaller than the conventional threshold for lasing  $\omega'_z \leq \Omega_U + \sqrt{4\eta^2(\gamma_{\uparrow} - \gamma_{\downarrow})/\kappa - \gamma_t^2/4}$ .

The lower polaritonic mode can be resonantly pumped when  $\eta = -\eta'$ . In this case, the effective damping for both modes have a minimum at the lower polariton frequency  $\Omega_L$ .

## Appendix F: Second cumulants

In models with collective, permutation-symmetric interactions, one can consider the leading effect of  $1/N$  corrections beyond mean-field, by including second-order connected correlation functions [79, 80]. In general, for finite values of  $N$ , all higher order connected correlations are relevant for dynamics; however, their effect is expected to be parametrically small in increasing powers of  $1/N$  (if  $N$  is large). This is at the root of the solvability of models with all-to-all interactions mediated by a common bosonic mode, as in our system: the BBGKY hierarchy [81, 82] closes when large system sizes are considered, allowing for non-perturbative solutions in the couplings governing both unitary or dissipative dynamics.

We include two-point connected correlation functions which couple to mean-field motion, neglecting third and higher order cumulants by approximating three point functions by their disconnected component

$$\langle ABC \rangle \simeq \langle AB \rangle \langle C \rangle + \langle AC \rangle \langle B \rangle + \langle BC \rangle \langle A \rangle - 2\langle A \rangle \langle B \rangle \langle C \rangle.$$

We simulate the dynamics and compare them with the mean-field solution to estimate the timescale,  $t_E$ , where cumulants have sufficiently grown to invalidate the mean-field description. We find that inside the L1 phase  $t_E$  scales as the square root of the number of spins (Fig. 9). After  $t_E$ , one would have to take into account higher order correlations to correctly predict the dynamics. At times  $t \sim \mathcal{O}(N)$  the dynamics of correlators undergoes phase diffusion [83, 84].

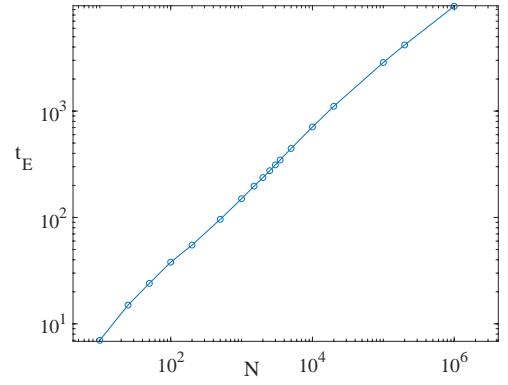


FIG. 9. Fit of the timescale  $t_E \propto N^{\delta}$  with  $\delta \simeq 0.5$ , as a function of number of spins in the system,  $N$ , within the lasing region. We extract  $t_E$  as the time when the ratio between second cumulants and mean-field expectation values becomes of order  $\sim 0.1$ .

### Appendix G: Difference between L1 and L2 regions

In this Section we consider how the transition between phases L1 and L2 is captured in dynamics of observables. As we pointed out in the main text, inside L1 region the dynamics have unbroken  $\mathbb{Z}_2$  symmetry. Spins components oscillate in time; the frequency of oscillations of  $\langle S^z \rangle$  is twice of the frequency of oscillations of  $\langle S^x \rangle$  and  $\langle S^y \rangle$ . These latter two observables have zero time average. By increasing  $\lambda$  above  $\lambda_c$ , the time-averaged value of  $\langle S^x \rangle$  becomes finite  $\langle S^x \rangle_t = \pm s_0^x$  while the amplitude of oscillations decreases. In Fig. 10(a) the amplitude of oscillations (solid line) and absolute value of the time averaged  $\langle S^x \rangle$  (dashed line) are plotted as functions of  $\lambda$ . In Fig. 10(b) trajectories of  $\langle S \rangle$  for different values of  $\lambda$  are shown. Note that for  $\lambda > \lambda_c$ , depending on initial conditions, one of two trajectories (red or blue lines) are possible with time averaged  $\langle S^x \rangle_t = \pm s_0^x$ , respectively.

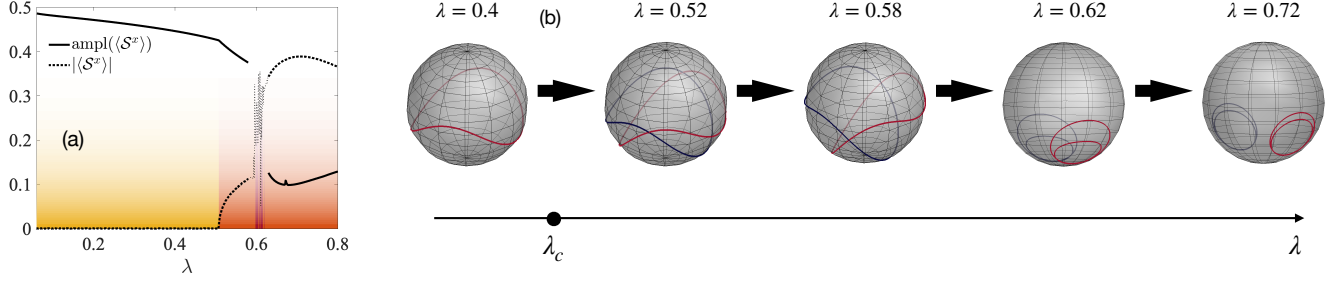


FIG. 10. (a) Amplitude of the oscillations of the  $\langle S^x \rangle$  (solid line) and absolute value of the time-averaged  $\langle S^x \rangle$  (dashed line) as function of  $\lambda$ . We choose all parameters as in Fig. 2 and fixed  $\gamma_\uparrow = 0.9$ . The colors are the same as in Fig. 2. Yellow, orange and red colors correspond to L1, L2 and IR phases, respectively. (b) Dynamics of the spin  $\langle S \rangle$  on the Bloch sphere inside L1 and L2 regions for different values of  $\lambda$ . Note that inside L2 region, depending on the initial conditions, one of two trajectories is possible with opposite time-averaged values of  $\langle S^x \rangle_t = \pm s_0^x$ .